Cement & Concrete Composites 43 (2013) 78–85

Contents lists available at ScienceDirect

Cement & Concrete Composites

journal homepage: www.elsevier.com/locate/cemconcomp

Nanosilica effects on composition and silicate polymerization in hardened cement paste cured under high temperature and pressure

Jung J. Kim [a], Muhammad K. Rahman [b], Abdulaziz A. Al-Majed [c], Mesfer M. Al-Zahrani [d], Mahmoud M. Reda Taha [e,*]

[a] Green Infrastructure Technology for Climate Change Research Center, Yonsei University, Seoul 120-749, South Korea
[b] Center for Engineering Research, Civil Engineering Department, King Fahd University of Petroleum & Minerals, Dhahran 31261, Saudi Arabia
[c] Department of Petroleum Engineering, King Fahd University of Petroleum & Minerals, Dhahran 31261, Saudi Arabia
[d] Civil Engineering Department, King Fahd University of Petroleum & Minerals, Dhahran 31261, Saudi Arabia
[e] Department of Civil Engineering, University of New Mexico, Albuquerque, NM 87131, United States

ARTICLE INFO

Article history:
Received 12 September 2011
Received in revised form 12 June 2013
Accepted 6 July 2013
Available online 18 July 2013

Keywords:
Nanosilica
Microstructure
XRDA
NMR
Nanoindentation

ABSTRACT

Cement pastes of water to cement ratio (w/c) of 0.45 with and without nanosilica are hydrated under two conditions, room condition (20 °C with 0.1 MPa pressure) and an oil well condition (80 °C with 10 MPa pressure) for 7 days. For the cement pastes with nanosilica, 1% and 3% of cements weights were replaced by nanosilica. The composition of the hardened cement pastes is investigated using X-ray diffraction (XRD). Nuclear magnetic resonance (NMR) experiments are used to quantify the silicate polymerization in hydrated cement paste. Microstructural phases are identified according to the corresponding mechanical property using nanoindentation. The results showed that under room curing conditions, hardened cement paste with 1% nanosilica has the highest level of calcium silicate hydrate (C–S–H) polymerization. However, under high temperature and pressure curing conditions, hardened cement paste with 3% nanosilica has the highest level of C–S–H polymerization. A new relatively stiff microstructural phase is observed in cement pastes incorporating nanosilica and cured under elevated pressure and temperature conditions. The significance of curing conditions and nanosilica content on the polymerization and stiffness of hydrated cement pastes are discussed.

1. Introduction

The 2010 fracture of oil wells in the Gulf of Mexico and the associated environmental impact with the loss of billions of oil barrels necessitates investigation to produce reliable and durable cementing materials for oil well operations. Producing sustainable oil wells is a major concern for countries with large oil production like the Kingdom of Saudi Arabia (KSA). KSA has 267 billion barrels of proven oil reserves with 100 major oil and gas fields and more than 1500 active oil wells. Many of these reserves are relatively deep and maintain high temperatures with elevated pressure.

In oil and gas well drilling operations, the cementing of well casing is typically performed by incorporating oil well cement (OWC) slurry to aid in the drilling process. The composite system formed is vital for precluding a host of undesirable processes which can severely impact the production process. Stringent performance requirements are therefore placed on the cement slurries used, including low viscosity, rapid strength development, low permeability and enhanced resistance to aggressive fluids. A number of recent research investigations have been conducted to develop high performance OWC [1–3], however, only limited results are available. It is important to note that OWC is very similar in composition to Type I, Type II and Type I/II ordinary Portland cements (OPC) while incorporating limited amount of fluidity admixtures [4].

The major cement hydration product that makes up approximately 67% of hydrated OPC paste is calcium–silicate–hydrate (C–S–H) [5]. It is suggested that C–S–H, which consists of nano-structured colloidal layers, can be altered by incorporating nanoparticles such as nanosilica and nanoalumina. Recent studies have shown that a great potential exists to improve the mechanical characteristics of cement paste by incorporating nanosilica, nanoalumina and carbon nanotubes [6–8]. Developments in nanotechnology over the past few years have paved several avenues for development of new materials that can alter properties of cement mortar and concrete. Early efforts in nanotechnology were directed to understand the fundamental phenomena of cement hydration and cement degradation mechanisms [9]. Studies in nano-modified cements, self-healing cement and other nano-based cementitious materials have been in progress for the last decade [10]. It has been shown by several researchers that traditional cement based

* Corresponding author. Tel.: +1 505 277 1258; fax: +1 505 277 1988.
E-mail address: mrtaha@unm.edu (M.M. Reda Taha).

0958-9465/$ - see front matter © 2013 Elsevier Ltd. All rights reserved.
http://dx.doi.org/10.1016/j.cemconcomp.2013.07.002

materials showed radically enhanced properties when engineered at the nanoscale [11]. Moreover, nanoparticles such as TiO_2, ZnO_2, fullerenes, carbon nanotubes, silica, alumina, magnesium, calcium and clays have been examined to alter strength, stiffness and ductility characteristics of cementitious materials [8,11].

In this study, a basic science investigation was conducted with the objective of understanding the significance of elevated temperature and pressure curing conditions on the hydration of OPC in the presence of nanosilica. OPC cement pastes with water to cement ratio (w/c) 0.45 without and with nanosilica contents of 1% and 3% are hydrated for 7 days under two conditions: room condition of 20 °C and 0.1 MPa pressure and an elevated condition of 80 °C with 10 MPa pressure. Type II OPC was used for its resemblance to OWC composition specifically with respect to C–S–H hydration. Using ^{29}Si magic angle spinning (MAS) nuclear magnetic resonance (NMR), the silicate polymerization of hydrated cement is investigated. The microstructural compounds in the hardened cement pastes are also investigated by X-ray diffraction (XRD) analysis. The mechanical characteristics of the microstructural phases in the hardened cement pastes represented by the modulus of elasticity are investigated using nanoindentation. The results shed light on the significance of curing conditions on the hydration products.

2. Methods

2.1. X-ray diffraction (XRD)

XRD is a well-known methodology in cement chemistry [12] and is used to detect various compounds in a cement paste. XRD is usually used to characterize crystalline materials. Using XRD spectra, several compounds in hydrated cement paste such as tricalcium silicate (C_3S), dicalcium silicate (C_2S), ettringite (AFt), calcium hydroxide (CH) and calcium silicate hydrate (C–S–H), can be detected. There exists a wealth of information in the literature on XRD observations of cement hydration products [12–14].

2.2. ^{29}Si magic angle spinning nuclear magnetic resonance (^{29}Si MAS NMR)

Silicate polymerization represents the number of bonds generated by the silicate tetrahedron. The description of a silicate tetrahedron with various sharing oxygen atoms is shown in Fig. 1. A silicate tetrahedron having the number of n sharing oxygen atoms is expressed as Q^n where n is the number sharing oxygen atoms ranging from zero to four. As described in Fig. 1, Q^0 is observed due to the remaining C_3S and C_2S in hydrated cement while Q^1 (end-chain group), Q^2 and Q^3 (middle-chain group) in silicate are typically detected due to the layered structure of C–S–H. Q^4 is the polymerization of the quartz and can be observed in silica rich products such as fly ash and silica fume. The intensity of the silicate Q connections can be investigated using ^{29}Si MAS NMR technique. Using the intensity fractions of Q^ns, the degree of hydration D_h of a hydrated cement paste can be calculated as [15]

$$D_h = I_Q^1 + I_Q^2 + I_Q^3 \tag{1}$$

where I_Q^n represents the corresponding intensity of Q^n connection respectively. If a silica rich material is used for a hydrated cement paste, the pozzolanic activity coefficient D_{pa} is calculated by comparing the intensity fraction of Q^4 at time t_0 and t as [1]

$$D_{pa} = \frac{I_Q^4(t) - I_Q^4(t_0)}{I_Q^4(t_0)} \tag{2}$$

The average degree of C–S–H connectivity D_c, which can represent the silicate polymerization, in a hydrated cement paste is also calculated as [1]

$$D_c = \frac{I_Q^1 + 2I_Q^2 + 3I_Q^3}{I_Q^1 + I_Q^2 + I_Q^3} \tag{3}$$

High values of D_c represent high polymerization of C–S–H. From the extensive studies of the structure of C–S–H by ^{29}Si MAS NMR, it was shown that the polymerization of C–S–H depends on its compositional C/S ratio (high polymerization for low C/S ratio) and the humidity in interlayer water (high polymerization for low interlayer water) [15,16].

The relative quantity of sharing oxygen atoms of a silicate tetrahedron in a silicate material can be detected by ^{29}Si MAS NMR and this information is used to interpret the polymerization of a silicate tetrahedron. The typical chemical shift peaks for Q^0, Q^1, Q^2, Q^3 and Q^4 appeared in hydrated cement are near −74, −80, −84, −95 and −110 (pozzolanic silica), respectively [1,17]. As '*the next nearest neighbor*' of a silicate tetrahedron can affect chemical shift, the chemical shifts for silicate tetrahedral are varied. The ^{29}Si chemical

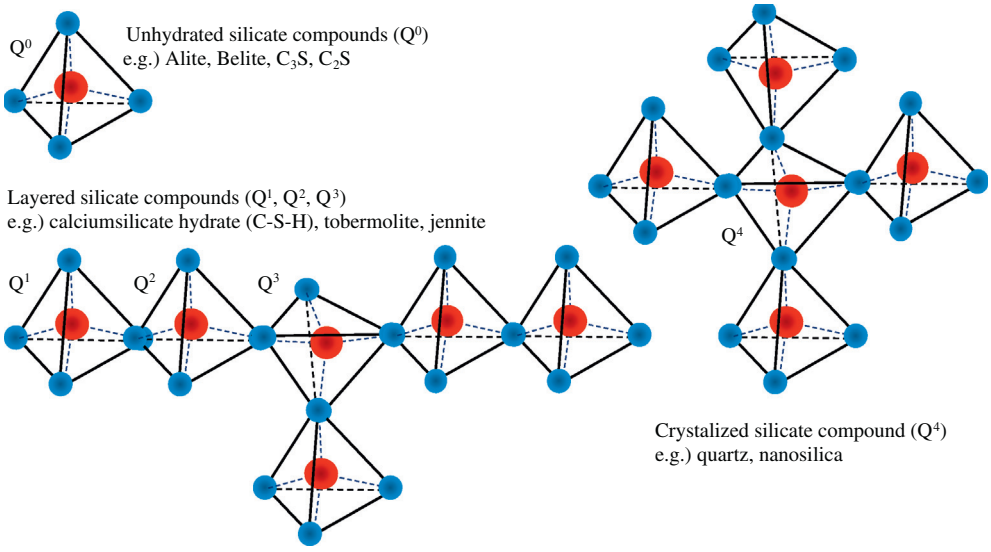

Fig. 1. Silicate connections.

shifts are respectively referenced relative to tetramethylsilane $Si(CH_3)_4$ (TMS) at 0 ppm, using $Si[(CH_3)_3]_8Si_8O_{20}$ (Q8M8) as a secondary reference (the major peak being at 11.6 ppm relative to TMS).

2.3. Nanoindentation

Nanoindentation experiments of hydrated cement pastes were able to identify several microstructural phases in hydrated cement such as CH, C–S–H and unhydrated cement (C_3S, C_2S). These phases can be identified based on their modulus of elasticity [18]. Moreover, two nanoscale phases can be observed in C–S–H, namely low density (LD) and high density (HD) C–S–H that were reported by others [18,19]. Analysis of the nanoindentation data to extract elastic modulus is performed after the Oliver and Pharr method [20]. This method [20] recognized that the unloading curve for a majority of indented materials followed a power curve fit rather than a linear relationship. Therefore, a power function can be used to fit the top 60% of the unloading curve and the slope of indentation load-depth curve (dP/dh) can be calculated as the derivative of the power fit curve. The reduced modulus, E^* is calculated as Eq. (4) after [20] and [21]:

$$E^* = \frac{1}{2\beta}\frac{\sqrt{\pi}}{\sqrt{A}}\frac{dP}{dh} \tag{4}$$

where β is a correction factor to account for the non-symmetrical shape of the indenter tip, which is equal to 1.034 for a 3-sided pyramidal (Berkovich) indenter. A is the contact area of the indenter, which is found by knowing the geometry of the indenter tip as a function of the depth, and the measured depth. For a Berkovich indenter tip, A can be calculated as [21]:

$$A = 3\sqrt{3}h_p^2\tan^2\theta \tag{5}$$

where h_p is the depth of penetration and θ is the angle the edge of the indenter makes with the vertical. The reduced modulus E_r is used in lieu of Young's modulus to account for the affect of the indenter stiffness on measurements. The reduced modulus E_r is derived from Eq. (6), where v is Poisson's ratio and E is Young's modulus of the indented phases; E' and v' are values corresponding with the indenter frame equal to 1141 GPa and 0.07 respectively as reported by the indenter calibration.

$$\frac{1}{E_r} = \frac{1-v^2}{E} + \frac{1-v'^2}{E'} \tag{6}$$

The analysis can be extended to extract many other mechanical characteristics at the nanoscale including toughness, fracture toughness and creep [20]. The data is then analyzed using statistical methods to identify the volume fraction of the different microstructural phases after Constantinides et al. [18]. The statistical analysis targets placing each observation into a bin that describes one microstructural phase in the hydrated cement. The number of bins required can be calculated as $K = 3N - 1$, where N is the number of phases in the sample. An experimental density function (*EDF*) is calculated as $(f/K)/M$, where f is the frequency, K is the bin size, and M is the number of data points. The data is then fit to individual probability density functions (*PDFs*), where each phase is represented by its own *PDF* calculated as Eq. (7):

$$p_i(x) = \frac{f_i}{\sigma_i\sqrt{2\pi}}e^{-\left(\frac{(x-\mu_i)^2}{2\sigma_i^2}\right)} \tag{7}$$

Here μ_i is the average value, σ_i is the standard deviation and f_i is the frequency represented by the surface fraction occupied by the i-th phase on the indentation surface. The error between points of the *EDFs* and points of the *PDFs* can be calculated. The optimal microstructural phase identification is the one that minimizes the error between the *EDFs* and *PDFs*.

3. Experiments

3.1. Materials

A comparison of the chemical composition of Class G and Class H OWC with typical Type II OPC, known as low temperature and sulfate resistance cement [4,22] is presented in Table 1. While an obvious difference in aluminate (C_3A) content can be observed, the difference in the major clinker product responsible for forming C–S–H represented by C_3S and C_2S is almost negligible. The difference is therefore not related to strength but to the speed of cement hydration and hydration temperature which are key requirements for OWC [13]. The low content of C_3A in Class G and Class H OWC is also essential for limiting the amount of ettringite in hydrated cement which is a key requirement for sulfate resistance [14,23]. Therefore, C–S–H, the major hydration product in cement responsible of strength, fracture and durability in Class G and Class H OWC is very similar to that produced using Type II OPC [12]. The decision to use Type II OPC stemmed from the need to avoid the effect of any possible fluidity additives, typically incorporated in OWC, on the hydration products at elevated temperature and pressure conditions.

The nanosilica used is AEROSIL® 380, which has average BET surface area of 380 m^2/g and average particle diameter of 7 nm. w/c of 0.45 was used for all cement paste specimens. For XRD, NMR and nanoindentation of cement paste, two cylinders, ϕ 10 mm × 10 mm height, were prepared for each type mix. The procedures for mixing the hydraulic cement pastes followed the ASTM standards [24]. The specimens were molded in a tube for a day and then cured in the corresponding curing condition. Although a special technique to disperse nanosilica was not necessary with the 1% and 3% nanosilica content used to make ϕ 10 mm × 10 mm specimens in this study, special dispersion methods might be necessary with large nanosilica content or large patch sizes to ensure high pozzolanic reactivity. Nanosilica contents and curing conditions are presented in Table 2. The rationale behind selecting the curing period conditions was to simulate field conditions of oil well cement based on published literature [1,25,26].

3.2. Curing set-up

For room curing conditions, specimens were cured under tap water with a controlled temperature of 20 °C and pressures 0.1 MPa (1 atm). For elevated temperature and pressure curing conditions similar to deep oil well condition, a special set-up for the elevated temperature of 80 °C and pressure of 10 MPa (98.7 atm) was prepared as shown in Fig. 2. 450 ml *Parr*® pressure

Table 1
Synthetic C-S-H slurry compositions from TGA analysis results and the stoichiometric formula of the synthetic C-S-H estimated from TGA results.

C/S	Mass loss (145 °C~350 °C)	[a]C/S	[a]x	Mass loss (350 °C~500 °C)	CH content	Mass loss (600 °C~825 °C)	$CaCO_3$ content
0.9	7.895%	0.73	0.55	2.486%	10.2%	0.443%	1.0%
1.2	9.81%	1.0	0.8	2.503%	10.3%	0.527%	1.2%
1.5	22.12%	1.24	2.42	2.334%	9.6%	1.035%	2.4%

[a] Molecular weights of 74.10, 18.01, 44.01 and 100.09 g/mol are used for CH, H_2O, CO_2, $CaCO_3$ respectively.

Table 2
Nanosilica contents and curing conditions.

Specimens	Pozzolans	Curing conditions		
		Temperature (°C)	Pressure	Time (days)
C-rm	Not added	20 °C	0.1 MPa (1 atm./15.2 psi)	7 days
N1%-rm	1% nanosilica	20 °C	0.1 MPa (1 atm./15.2 psi)	7 days
N3%-rm	3% nanosilica	20 °C	0.1 MPa (1 atm./15.2 psi)	7 days
C-hc	Not added	80 °C	10 MPa (98.7 atm./1 atm./1500 psi)	7 days
N1%-hc	1% nanosilica	80 °C	10 MPa (98.7 atm./1 atm./1500 psi)	7 days
N3%-hc	3% nanosilica	80 °C	10 MPa (98.7 atm./1 atm./1500 psi)	7 days

rm indicates room curing conditions
hc indicates high temperature and pressure curing conditions

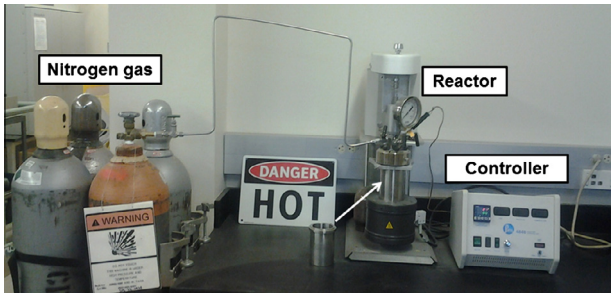

Fig. 2. Specimen curing set-up to simulate elevated temperature and pressure.

vessel was used. 300 ml of water filled the vessel and specimens were cured in the water under elevated temperature and pressure. Using the heater surrounding the vessel, temperature was elevated and kept constant during the curing time period. To prevent temperature fluctuations in the vessel, 20 °C cooling water was circulated through the cooling loop in the vessel. Pressure was applied by injecting nitrogen gas from a compressed Nitrogen cylinder at 10 MPa. In the discussion below "*rm*" is used to indicate room curing conditions and "*hc*" is used to indicate high temperature and pressure curing conditions.

3.3. Nanoindentation

Nanoindentation was performed using a Berkovich tip loaded at 0.55 mN including 0.05 mN preloading. Specimens were prepared for nanoindentation by first casting them in acrylic to fit them into the nanoindentation holder. The specimens were then polished on a Buehler Ecomet 3 polisher with a Buehler Automet 2 power head, which applied a constant pressure to the samples and provided additional spin on the samples for increased polishing efficiency. The steps used during polishing included: 10 min with a 125-μ diamond pad, 15 min with a 70-μ diamond pad, 15 min with a 30-μ diamond pad, 30 min with a 9-μ diamond lapping film pad, and 1 h with a 1-μ diamond lapping film pad. Fifty points were indented on each specimen and the results were analyzed to identify the elastic modulus of the different microstructural phases.

4. Results and discussion

4.1. Microstructural compositions by XRD spectra

The effects of nanosilica contents and different curing conditions on the cement hydration and pozzolanic activity were examined using XRD analysis. The XRD spectra were processed by Fast Fourier Transform (FFT) filter. The difference in the microstructure of the cement paste according to nanosilica contents 1% and 3% is compared in Fig. 3a for room curing conditions and Fig. 3b for elevated curing conditions. By comparing XRD spectra of 1% and 3% nanosilica added hydrated cement pastes cured in room conditions, quartz (nanosilica) peaks at 25.7°(2θ) appear in the XRD spectrum of cement paste incorporating 3% nanosilica while these peaks disappear in cement pastes incorporating 1% nanosilica as shown in Fig. 3a. It is evident from this analysis that most nanosilica contents beyond 1% remain unreacted at 7 day room curing conditions. This observation agrees with findings by others who reported the need to consider a threshold of nanosilica contents to enhance hydrated cement paste properties by pozzolanic reaction [8,27]. It is, however, important to note that unreacted nanosilica might produce a strain-softening like effect in the cement-nanosilica composite. Such behavior has been reported by nano-glass particles [28] and is yet to be investigated in cementitious materials. For the comparison of XRD spectra of hydrated cement pastes cured in elevated curing conditions (80 °C and 10 MPa), the quartz (nanosilica) peaks are not apparent in both cases as shown in

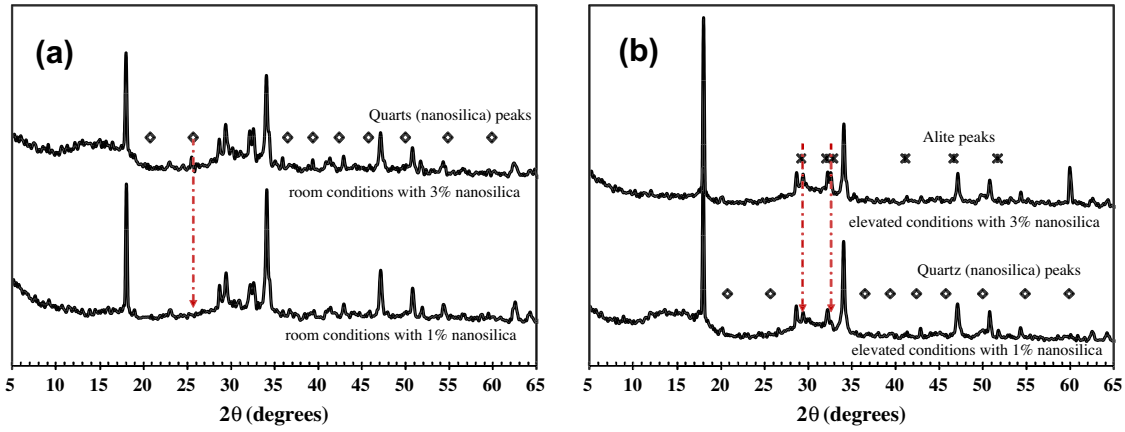

Fig. 3. (a) XRD spectra of 1% and 3% nanosilica pastes cured under room condition. (b) XRD spectra of 1% and 3% nanosilica pastes cured under elevated condition.

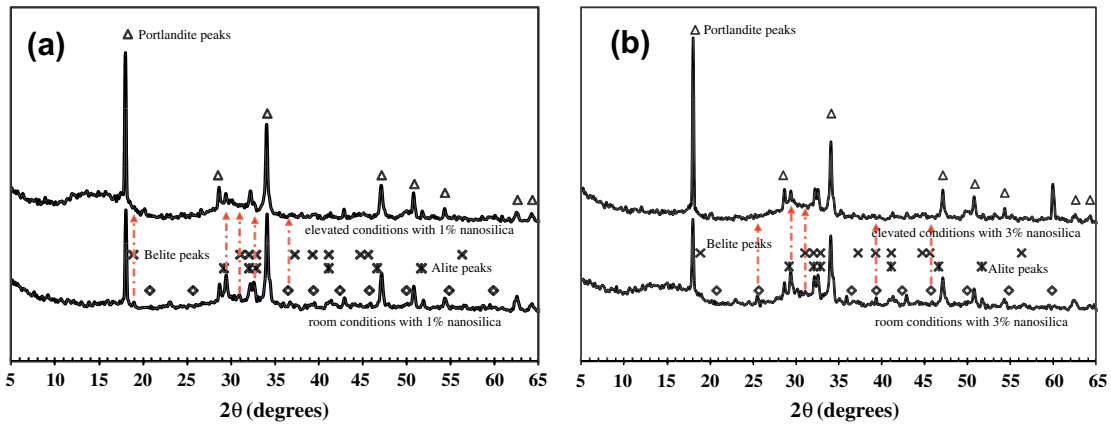

Fig. 4. (a) XRD spectra of 1% nanosilica pastes cured under room and elevated curing conditions. (b) XRD spectra of 3% nanosilica pastes cured under room and elevated conditions.

Fig. 3b. This indicates that most of the nanosilica particles are consumed in elevated curing conditions. It is also evident that more C_3S, known as the greatest contributor to early strength of cement paste, is consumed under elevated curing conditions when 3% nanosilica was incorporated to the cement paste. This is represented by the decrease in the alite XRD peaks at 29.2°(2θ) and 32.9°(2θ) in cement pastes incorporating 3% nanosilica compared with cement pastes incorporating 1% nanosilica as shown in Fig. 3b. Furthermore, the difference in microstructure as a result of the different curing conditions is compared in Fig. 4a for hydrated cement pastes incorporating 1% nanosilica and Fig. 4b for hydrated cement pastes incorporating 3% nanosilica. As shown in Fig. 4a, intense calcium hydroxide (CH) peaks at 18.2° (2θ) are apparent in the XRD spectrum of hydrated cement pastes incorporating 1% nanosilica in elevated curing conditions. Moreover, the quartz (nanosilica) peak at 36.5° (2θ) disappears in the XRD spectrum of hydrated cement pastes incorporating 1% nanosilica in elevated curing conditions. Furthermore, more C_3S and C_2S, known as most contributor for late strength of cement paste, are consumed under elevated curing conditions as alite peaks at 29.2° and 32.9° (2θ) and belite peaks at 18.9° and 31° (2θ) and decreases in specimens cured under elevated curing conditions. In Fig. 4b, a higher pozzolanic activity can be observed with elevated curing conditions for hydrated cement pastes incorporating 3% nanosilica. This observation is represented by the absence of the three quartz (nanosilica) peaks at 25.7°, 36.5° and 45.8° (2θ) from the XRD spectrum for hydrated cement pastes incorporating 3% nanosilica cured under elevated curing conditions. There is also evidence of more consumption of C_3S and C_2S in elevated curing conditions with the disappearance of peaks at 29.2° and 31° (2θ) respectively. The above observations confirm that the threshold of nanosilica contents for effective pozzolanic reaction seems to increase when the cement paste is cured under elevated temperature and pressure rather than under room condition. Moreover, it is evident that the hydration of cement paste is accelerated under elevated curing conditions based on the considerable increase in the consumption of alite and belite and the higher intensity of CH as shown in XRD spectra of hydrated cement paste specimens cured under these conditions. Further research will be needed to identify the optimal nanosilica content for curing under elevated temperature and pressure conditions.

Table 3
Integration of Q^n intensities by deconvolution of ^{29}Si MAS NMR.

Specimens	I_Q^n (%)					D_h (%)	D_{pa} (%)	D_c
	I_Q^0	I_Q^1	I_Q^2	I_Q^3	I_Q^4			
C-rm	44	36	20	–	–	56.0	–	1.36
N1%-rm	26	35	26	–	13	60.9	87.0	1.43
N3%-rm	33	31	22	–	14	53.2	86.2	1.42
C-hc	22	37	40	–	–	77.7	–	1.52
N1%-hc	21	35	35	4	6	73.2	94.1	1.57
N3%-hc	21	33	36	5	6	73.6	94.4	1.62

D_h is degree of hydration: Eq. (1).
D_{pa} is degree of pozzolanic activity: Eq. (2).
D_c mean silicate chain length: Eq. (3).

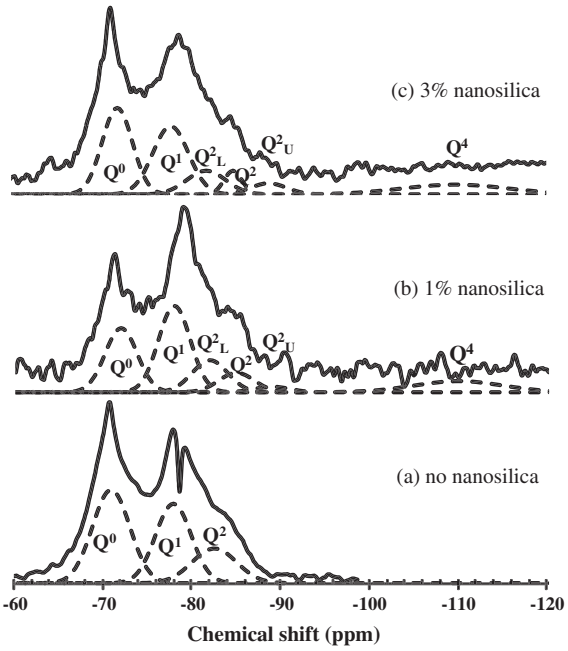

Fig. 5. NMR spectra of 0%, 1% and 3% nanosilica cured under room conditions.

4.2. Silicate polymerization analysis by NMR spectra

The resulting ^{29}Si MAS NMR spectra were deconvoluted and the effects of nanosilica and different curing conditions on the degree of hydration in Eq. (1), the pozzolanic activity in Eq. (2) and the degree of C–S–H connectivity in Eq. (3) were examined. The integration results of the Q^n intensities by deconvolution are presented in Table 3. The deconvoluted spectra for hardened cement without and with 1% and 3% nanosilica cured under room conditions are compared in Fig. 5 while those cured under elevated conditions are compared in Fig. 6. It is noticeable that Q^3 level of polymerization, which can be observed in tobermorite or jennite, was found in

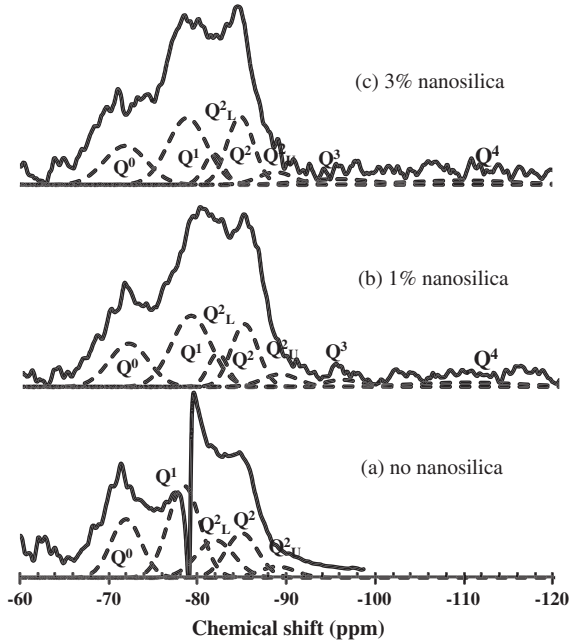

Fig. 6. NMR spectra of 0%, 1% and 3% nanosilica cured under elevated conditions.

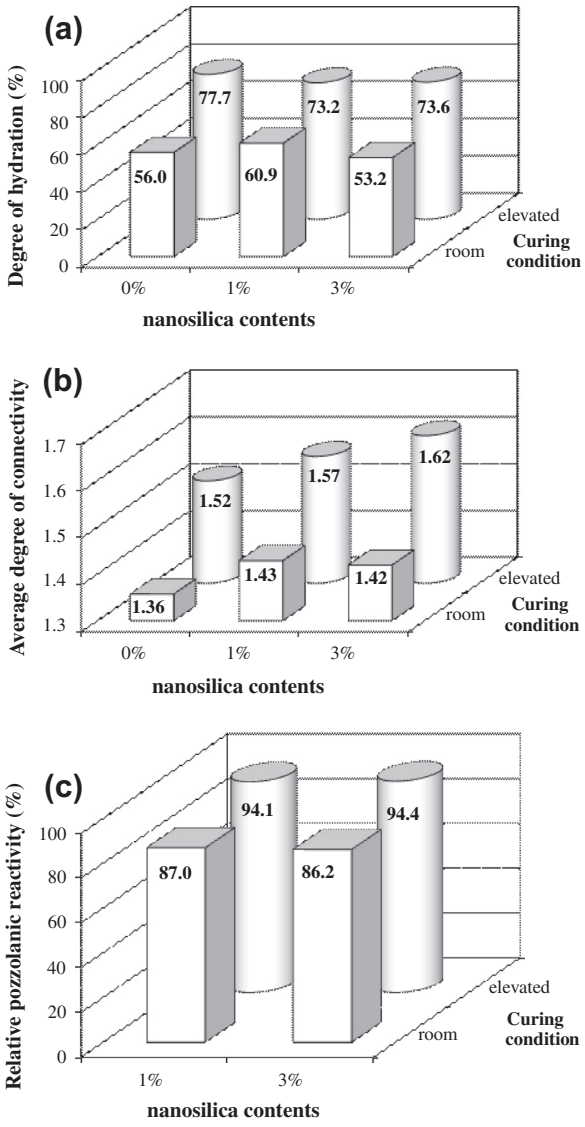

Fig. 7. Comparison of (a) the degree of hydration, (b) polymerization and (c) pozzolanic reaction according to nanosilica contents and curing conditions.

hardened cement with 1% and 3% nanosilica cured under high temperature and pressure as shown in Fig. 6. The Q^4 level of polymerization was shown in hardened cement with 1% and 3% nanosilica under both curing conditions due to the unreacted nanosilica as shown in Figs. 5 and 6.

For the effects of nanosilica contents on the degree of hydration of cement as compared in Fig. 7a, the highest degree of hydration under room curing conditions was 60.9% and occurred with cement paste specimens incorporating 1% nanosilica. However, the highest degree of hydration under elevated curing conditions was 77.7% and occurred with cement paste specimens without nanosilica. For the average degree of connectivity (polymerization) as compared in Fig. 7b, the highest degree of polymerization of 1.62 occurred with cement paste specimens incorporating 3% nanosilica cured under elevated curing conditions. The highest degree of connectivity under room curing conditions of 1.43 occurred with cement paste specimens incorporating 1% nanosilica. These observations confirm the aforementioned findings by XRD analysis that the threshold of nanosilica content is significantly affected by the curing conditions. There is a significant increase in the beneficial nanosilica threshold when cement is cured under elevated temperature and pressures. Such high content of nanosilica is able to significantly increase the degree of silicate polymerization of hydrated cement paste cured under elevated conditions.

The relative pozzolanic activity is calculated using Eq. (2). As the initial Q^4 value is not available, a unity is used for that value. The relative pozzolanic activity is compared in Fig. 7c. It can be observed that the relative pozzolanic activity significantly increased under elevated curing conditions compared with room curing conditions. However, there is no significant difference in the relative pozzolanic activities due to increasing the nanosilica content from 1% to 3% under both curing conditions. Therefore, one can conclude that there can be a significant enhancement in the quality of the hydration products, strength and reduced permeability if high content nanosilica is used under high temperature and pressure curing conditions such as in oil wells. There is evidence that contents beyond 1% nanosilica are being consumed under these curing conditions, but the optimal content of nanosilica under these conditions needs to be identified. Further research is warranted to correlate these findings to other macroscale strength and durability characteristics of hydrated cement paste with and without nanosilica.

4.3. Mechanical characterization by nanoindentation spectra

A total of 50 indentations were performed for each hydrated cement paste. The indentations were performed in five rows with ten indentations spaced at 200 μm on each row. The distribution of the modulus of elasticity is deconvoluted using the method described above (Eqs. (4)–(7)) and the results are summarized in Table 4. The degree of hydration was calculated based on the identified volume fraction of unhydrated cement particles. While microstructural phases identified from our nanoindentation experiments were reported by other researchers [29–31], the analysis indicated one unknown relatively stiff phase that was not reported in the literature before. This unknown phase appeared only in the cement paste incorporating nanosilica cured under elevated curing conditions as shown in Table 4. When this relatively stiff 'new phase' in Table 4 is considered, the degree of hydration calculated from nanoindentation results agrees well with that extracted from ^{29}Si MAS NMR. This observation suggests that there might be more

Table 4
Microstructural phase fractions from deconvolution of nanoindentation results.

Phases *E* range (GPa)	Ettringite 4–6 (%)	LD-CSH 18–21 (%)	HD-CSH 28–31 (%)	CH 39–43 (%)	New phase 52–59 (%)	Unhydrated cement particle 1 53–62 (%)	Unhydrated cement particle 2 82–119 (%)
C-rm	2	23	15	18	–	34	8
N1%-rm	4	20	25	20	–	23	8
N3%-rm	2	16	20	21	–	33	8
C-hc	2	39	18	21	–	14	6
N1%-hc	4	8	12	24	26	–	26
N3%-hc	4	14	20	28	8	–	26

rm is room curing conditions.
hc is high temperature and pressure curing conditions.

sub-microstructural phases than those reported in the literature to be realized using nanoindentation for cement pastes incorporating nanosilica and cured under high temperature and pressure curing conditions.

For the cement pastes cured in elevated conditions for 7 days, LD–C–S–H occupies close to half of the hydration products of the cement paste without nanosilica (C-hc in Table 4) while the LD–C–S–H fraction in hydration products of the cement paste incorporating nanosilica decreases significantly and a stiff 'new phase' appears (N1%-hc and N3%-hc in Table 4). Nanoindentation experiments [32] elucidated the relationship between packing density and modulus of elasticity of C–S–H. Considering this relationship and colloidal interpretation of C–S–H [33,34], it can be hypothesized that the microstructural phases such as LD–C–S–H (packing density 0.63) can be condensed to HD–C–S–H (packing density 0.76) or very high density (packing density over 0.76) C–S–H under high temperature and pressure curing conditions and with the presence of a rich silica environment (i.e. high content of nanosilica). This might explain the formation of the relatively stiff 'new phase' under these conditions. Moreover, the presence of silicate tetrahedral connectivity of Q^3 in the cement paste incorporating nanosilica under elevated curing conditions in Fig. 6b and (c) supports this hypothesis as Q^3 has been observed in tobermorite which is known to be crystalline and has relatively high density [35]. Therefore, such high density C–S–H might be generated in a cement paste incorporating nanosilica under high temperature and high pressure. Further research is warranted at the macroscale to identify the significance of such high levels of silicate connectivity and relatively stiff microstructural phases on the strength and fracture toughness of hydrated cement pastes with nanosilica and elevated curing conditions.

5. Conclusion

The microstructural compositions and the silicate polymerization of the cement pastes without and with 1% and 3% nanosilica hydrated under two curing conditions, 20 °C with 0.1 MPa pressure and 80 °C with 10 MPa pressure, for 7 days were examined using XRD, ^{29}Si MAS NMR and nanoindentation. It is evident that the hydration of cement paste is faster under elevated curing conditions than under room curing conditions. The results also showed that the nanosilica fraction participating in the pozzolanic reaction increased when the cement paste is cured under elevated temperatures and pressures rather than those done under room conditions.

While 1% nanosilica was able to produce significant silicate polymerization under ambient curing conditions, 3% nanosilica increased silicate polymerization considerably under elevated curing conditions. We expect that nanosilica content higher than 3% might be necessary to further increase the degree of silicate polymerization of hydrated cement paste cured under higher temperature and pressure than those reported in this study. These findings can be of significant value for oil well operations where elevated temperature and pressure curing conditions might improve the quality of the cement lining if relatively high nanosilica content (about 3%) is used. Moreover, the observation of a relatively stiff hydration product, denoted as 'new phase' in this study, suggests that there might be other sub-microstructural phases of C–S–H than those earlier reported in the literature. Such phases can be observed by nanoindentation of cement pastes incorporating nanosilica and cured under elevated curing conditions. Further research is warranted to correlate these nano and microstructure findings to macroscale characteristics of these hydrated cements.

Acknowledgements

The authors would like to acknowledge the support provided by King Abdulaziz City for Science and Technology (KACST) through the science and technology unit at King Fahd University of Petroleum and Minerals (KFUPM) for funding this work through Project #09-NAN754-04 as part of the National Science, Technology and Innovation Plan. Additional funding to the first author by the National Research Foundation of Korea (NRF) grant funded by the Korea government (MEST) (No. 2011-0030842) is greatly appreciated. The corresponding author appreciates funding by National Science Foundation (NSF), USA award # 1131369.

References

[1] Le Saoût G, Lécolier E, Rivereau A, Zanni H. Chemical structure of cement aged at normal and elevated temperatures and pressures. Part II: Low permeability class G oilwell cement. Cem Concr Res 2006;36:428–33.
[2] Jansson I, Skarp U, Bigley CH. The value of colloidal silica for enhanced durability in high fluidity cement based mixes. Paper presented at: Fifth international symposium on self-compacting concrete. Ghent, Belgium; 2007.
[3] Lal K, Meher RK, Rautela RS, Dasgupta D. Pozzolans – Portland cement: an alternate to API oil well cement. Paper presented at: PetroTech, New Delhi, India; 2009.
[4] API. API specification for materials and testing for well cements. API Specification 10: API; 1990.
[5] Taylor H. Nanostructure of C-S-H: current status. Adv Cem Based Mater 1993;1:38–46.
[6] Kuo W-Y, Huang J-S, Lin C-S. Effects of organo-modified montmorillonite on strengths and permeability of cement mortars. Cem Concr Res 2006;36:886–95.
[7] Li Z, Wang H, He S, Lu Y, Wang M. Investigations on the preparation and mechanical properties of the nano-alumina reinforced cement composite. Mater Lett 2006;60:356–9.
[8] Mondal P, Shah SP, Marks LD, Gaitero JJ. Comparative study of the effects of microsilica and nanosilica in concrete. J Transp Res Board: Nanotech Cem Concr 2010;1(2141):6–9.
[9] Scrivener K, Kirkpatrick RJ. Innovation in use and research on cementitious material. Cem Concr Res 2008;38:128–36.
[10] Chaipanich A, Nochaiyaa T, Wongkeoa W, Torkittikul P. Compressive strength and microstructure of carbon nanotubesnext term–fly ash previous term cement next term composites. Mater Sci Eng A 2010;527(4–5):1063–7.
[11] Sanchez F, Sobolev K. Nanotechnology in concrete – A review. Constr Build Mater 2010;24(11):2060–71.
[12] Taylor HFW. Cement chemistry. vol 1. 2nd ed. London: Thomas Telford Publishing; 1997.
[13] Mehta K, Monterio PJM. Concrete: Microstructure, Properties and Materials. 3rd ed. NY (USA): McGraw-Hill Professional; 2006.

[14] Diamond S. Cement paste microstructure–an overview at several levels. Paper presented at: Hydraulic cement pastes; their structure and properties. Tapton Hall, University of Sheffield; 1976.
[15] Bell GMM, Benstedm J, Glasser FP, Lachowski EE, Roberts DR, Taylor MJ. Study of calcium silicate hydrates by solid state high resolution 29Si nuclear magnetic resonance. Adv Cem Res 1990;3:23–37.
[16] Cong X, Kirkpatrick RJ. 29Si MAS NMR study of the structure of calcium silicate hydrate. Adv Cem Based Mater 1996;3:144–56.
[17] Alizadeh R. Nanostructure and engineering properties of basic and modified calcium-silicate-hydrate systems. Ottawa: Department of Civil Engineering, University of Ottawa; 2009.
[18] Constantinides G, Ulm F, et al. On the use of nanoindentation for cementious materials. Mater Struct 2003;36(April):191–6.
[19] Ulm F-J, Vandamme M, et al. Does microstructure matter for statistical nanoindentation techniques? Cem Concr Compos 2009;32.
[20] Oliver W, Pharr G. An improved technique for determining hardness and elastic modulus using load and displacement sensing indentation experiments. J Mater Res 1992;7(6):1564–83.
[21] Fischer-Cripps AC. Nanoindentation. New York: Springer Science+Business Media, LLC; 2004.
[22] ASTM-C150. Standard Specification for Portland Cement. USA: ASTM; 2009.
[23] Neville AM, Brooks JJ. Concrete Technology, vol. 1. Singapore: Longman Singapore Publishers Ltd; 1987.
[24] ASTM-C305. Standard Practice for Mechanical Mixing of Hydraulic Cement Pastes and Mortars of Plastic Consistency. West Conshohocken (PA): ASTM International; 1999.
[25] Scherer GW, Funkhouser GP, Peethamparan S. Effect of pressure on early hydration of class H cement. Cem Concr Compos 2010;40:845–50.
[26] Zhang J, Weissinger EA, Peethamparan S, Scherer GW. Early hydration and setting of oil well cement. Cem Concr Res 2010;40:1023–33.
[27] Kim JJ, Fan T, Reda Taha MM. Homogenization model examining the effect of nanosilica on concrete strength and stiffness. Transp Res Rec 2010;2141:28–35.
[28] Rao RB, Kobelev VL, Li W, Lewis JA, Schweizer KS. Nonlinear elasticity and yielding of nanoparticle glasses. Langmuir 2006;22:2441–3.
[29] Velez K, Maximilien S, et al. Determination by nanoindentation of elastic modulus and hardness of pure constituents of Portland cement clinker. Cem Concr Res 2001;31:555–61.
[30] Ulm F-J, Vandamme M, et al. Statistical indentation techniques for hydrated nanocomposites: concrete, bone, shale. J Am Ceram Soc 2007;90(9):2677–92.
[31] Mondal P, Shah SR, et al. Nanoscale characterization of cementitious materials. ACI Mater J 2008;105(2):174–9.
[32] Constantinides G, Ulm F. The nanogranular nature of C-S-H. J Mech Phys Solids 2007;55:64–90.
[33] Thomas JJ, Jennings HM. A colloidal interpretation of chemical aging of the C-S-H gel and its effects on the properties of cement paste. Cem Concr Res 2006;36:30–8.
[34] Powers TC, Brownyard TL. Studies of the physical properties of hardened Portland cement paste. PCA Bull; 1948.
[35] Alizadeh R, Beaudoin JJ. Mechanical properties of calcium silicate hydrates. Mater Struct 2011;44:13–28.